Enhancing LiDAR Data Positioning Accuracy in National Forest Surveys through Multi-Source Point Cloud Matching in Terrasolid software

Anna Shcherbacheva [1], Ana Puttonen [1], Arttu Soininen [1]

[1] Terrasolid LTD, Hatsinanpuisto 8. 02600, Espoo, Finland – anna.shcherbacheva@terrasolid.com, ana.puttonen@terrasolid.com, arttu.soininen@terrasolid.com

Keywords: point cloud processing software, LiDAR matching.

Abstract

National Land Surveys (NLS) worldwide extensively utilize LiDAR (Light Detection and Ranging) technology for forest inventory, integrating airborne (ALS) and terrestrial/mobile (TLS/MLS) LiDAR to obtain detailed 3D forest structure data. Efficient multi-modal data co-registration is essential for applications such as biomass estimation, forest volume assessment, growth monitoring, and tree mapping. Given the vast scale of NLS projects, often covering thousands of kilometres, efficient data processing is crucial. TerraScan provides two fully automated methods for co-registering TLS/MLS and ALS datasets: (1) signal marker-based registration and (2) tree stem-based registration. These methods achieve an average planimetric RMSE of 1.3–4.8 cm, offering state-of-the-art registration accuracy. The methods have been tested for robustness against ALS resolution deterioration, maintaining statistically similar performance even when point density is reduced to 26 pts/m². Also, the ALS data from National Land Survey (NLS) of Finland with 5-8 pts/m2 were tested and demonstrated the average co-registration RMSE comprising 7.5 cm. Optimized multi-threaded CPU processing enables rapid co-registration of massive datasets, making these methods highly suitable for large-scale national and global land surveys. Specifically, TerraScan tools enable the rapid co-registration of hundreds of millions of points within seconds.

1. Introduction

Forests are vital ecosystems that play a key role in regulating the global carbon cycle, maintaining climate stability, and preserving biodiversity. Covering approximately one-third of the Earth's land area, forests store substantial amounts of carbon, influence climate dynamics, and impact atmospheric greenhouse gas levels (Shestakova et al., 2016; Mori et al., 2017; Benson et al., 2020; Tian et al., 2023). Given their ecological significance, accurately capturing the three-dimensional structure of forests is a major scientific challenge. In recent years, Light Detection and Ranging (LiDAR) has become a preferred technology for forestry surveys due to its ability to penetrate dense vegetation and minimize external interference, enabling the efficient and precise acquisition of forest structural data (Pang et al., 2008; Guo et al., 2014; Liu et al., 2016).

In forest data acquisition, LiDAR technologies commonly include Terrestrial Laser Scanning (TLS) (Liang et al., 2018), Mobile Laser Scanning (MLS), and Airborne Laser Scanning (ALS) (Wehr et al., 1999). Ground-based LiDAR acquisition includes both Terrestrial Laser Scanning (TLS) and Mobile Laser Scanning (MLS), where the primary distinction lies in the platform's mobility. TLS operates from fixed positions, capturing high-resolution 3D data of tree trunks, understory vegetation, and lower canopy structures. In contrast, MLS utilizes a moving platform, such as a vehicle, to acquire LiDAR data continuously along a trajectory, improving efficiency over large areas. TLS/MLS, which operates from the ground level, excels at capturing detailed structural information on tree trunks and understory vegetation. However, the effectiveness of both TLS and MLS is constrained by canopy occlusion, limiting their ability to fully capture the upper canopy. Additionally, single-scan TLS data collection is often incomplete due to tree cover interference, necessitating multiple scans to achieve comprehensive coverage (Kelbe et al., 2015; Liu et al., 2017b; Zhang et al., 2021).

ALS, encompassing both manned and unmanned aerial vehicle laser scanning (ULS), offers a complementary approach by capturing structural information from above the canopy. It efficiently records canopy-level attributes such as tree height, crown width, and tree density, which are difficult to obtain using ground-based methods in dense forests (Kukkonen et al., 2021). ALS enables large-scale data collection in a short time, providing extensive coverage and high acquisition efficiency. However, its ability to penetrate dense canopies is limited, restricting the amount of information captured from lower forest layers (Paris et al., 2017; Liu et al., 2021). Moreover, differences in scanning perspectives and distances result in variations in the resolution and detail of ALS and TLS/MLS data, making them complementary rather than interchangeable for forest mapping. When these two data sources are co-registered, their compatibility enhances forest inventory accuracy by enabling the simultaneous extraction of individual-tree Diameter at Breast Height (DBH) from TLS or MLS and tree height from ALS, leveraging the strengths of each system.

Ensuring precise alignment of ALS and TLS/MLS point clouds is crucial for comprehensive forest mapping, encompassing tree trunks, canopies, and understory vegetation, while also maintaining consistency across platforms and over time, leading to more reliable forest assessments. Currently, two main approaches are used for point cloud registration. The first relies on auxiliary reference data, such as Global Navigation Satellite Systems (GNSS), artificial markers, or color images (Hohenthal et al., 2011; Yang et al., 2011; Pueschel et al., 2013; Abayowa et al., 2015; Avbelj et al., 2015; Zhang et al., 2016; Zhang et al., 2018). However, dense forest canopies present significant challenges for both artificial markers and GPS-based navigation systems. The thick foliage often obstructs artificial markers, making them difficult to detect or use as reference points for ground-based navigation. Additionally, dense canopies can block or attenuate satellite signals, leading to substantial GPS positioning errors. This issue is further compounded by multipath interference, where GPS signals are reflected off nearby objects such as tree leaves and branches, causing signal distortion and

large positional inaccuracies (Bastos and Hasegawa, 2013). For example, forest point clouds collected using TLS and MLS are often captured in a local coordinate system to prevent inaccuracies caused by unreliable GNSS conditions. Converting these datasets into a georeferenced coordinate system necessitates additional processing steps (Campos et al., 2024).

The second approach focuses on geometric feature-based alignment, providing a more data-driven and adaptable solution. Due to the intricate nature of forest structures, most studies rely on specific features as reference points during the registration process. These features include tree positions (Liang et al., 2013; Polewski et al., 2016; Liu et al, 2021), canopy height (Hauglin et al., 2014; Paris et al, 2017), canopy density (Dai et al., 2019; Zhou et al., 2023), tree trunk attributes (Liu et al., 2017a; Tremblay and Béland, 2018), and digital terrain models (Puletti et al., 2022). Notably, most existing LiDAR point cloud registration techniques have not been specifically developed or tested in highly complex environments with significant feature variability and a lack of external reference data (Castanheiro et al., 2023; Cheng et al., 2024) and suffer low accuracy and poor applicability.

Most geometric feature-based forest point cloud registration methods use a coarse-to-fine strategy. Liang and Hyyppä (2013) pioneered the use of tree stems for LiDAR registration, achieving robust results in boreal forests. Hauglin et al. (2014) improved this by matching TLS and ALS data using tree positions and size attributes, achieving 0.5–1 m accuracy. Polewski et al. (2016) introduced a stem descriptor based on tree distances, achieving 66 cm accuracy without requiring external GNSS data. Later, Polewski et al. (2019) enhanced this method with a weighted graph matching approach, further improving robustness.

Other studies explored canopy features. Liu et al. (2021) used canopy height and crown centers for TLS-UAV registration, achieving 43 cm accuracy. Shao et al. (2022) and Zhou et al. (2023) utilized canopy shapes and gaps, achieving 15 cm accuracy after fine-tuning with ICP. Pohjavirta et al. (2022) combined stem and ground points for TLS-UAV registration, achieving 7.2–13.6 cm accuracy in boreal forests.

Recent advancements include semantic key point detection (Dai et al., 2022) and hierarchical clustering with Fast Point Feature Histogram (FPFH) (Chen et al., 2024), achieving 29 cm and 15 cm accuracy, respectively. Overall, stem-based methods remain highly effective, with coarse registration typically achieving 10–50 cm accuracy, while fine registration often improves results to <15 cm.

In this study, we introduce two advanced co-registration methods implemented in Terrasolid software:

1) Artificial Markers – A traditional approach that leverages predefined markers for precise alignment.

2) Tree-Based Registration – A method inspired by the Markov Chain Monte Carlo (MCMC) sampling technique. This approach optimizes translation and rotation transformations by sampling tree stem pairs from ALS data, ensuring accurate alignment of detected tree stems.

Both methods benefit from the software automation, which pre-classifies ALS points into ground, low, medium, and high vegetation with subsequent tree stem detection. This detection accounts for the systematic distribution of ground points beneath individual tree canopies. Additionally, its highly optimized multi-threaded CPU processing enables the rapid co-registration of hundreds of millions of points within seconds.

2. Datasets

The datasets were obtained from a conifer-dominated boreal forest situated at Jämsänkoski Forest Institute (61°92’N, 25°10’E). The MLS data on scanning area of 130 m x 126 m was acquired by FARO Orbis (wavelength comprised 905 nm) scanner on 20th of August 2024. The Orbis delivers high-speed data acquisition with a precision of 5 mm in mobile mode and 120 m scanning range. The resulting point cloud contains 72,824,331 points with point density comprising 4,626 pts/m2.

The ALS data for scanning area of 317 m × 239 m were collected from UAV platform using YellowScan Mapper operated at 905 nm wavelength. The system consists of YellowScan Mapper scanner, high-precision GNSS receiver integrated onto a UAV platform, and RGB camera and a flight computer recording LiDAR and GNSS, data for post-processing. Georeferencing of the scanned area was carried out using 5 Ground Control Points (GCPs) by bundle block adjustment with mean Root Mean Square Error (RMS) error comprising 0.014 m. The resulting point cloud contained 66,046,344 points and featured 557 pts/m2 point density. The handheld scanner covered a subset of this region, located within the ALS-scanned area, see Figure 1. Figure 2 displays the point clouds obtained from both scanning platforms.

In addition, a bigger area scanned by NLS of Finland (0.69 x 0.52 km) with a density of 5 pts/m2 was used for testing, as shown in Figure 2(c), containing 5,910,452 points.

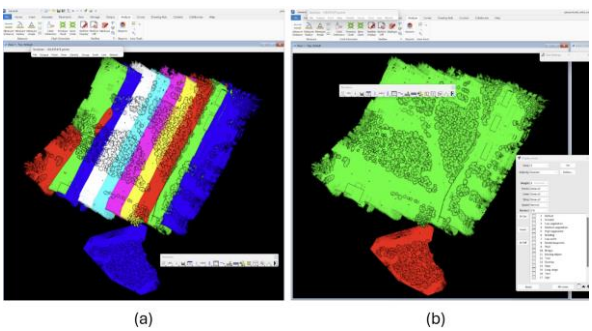

Figure 1. (a) Regions scanned with FARO Orbis (blue bottom region) and YellowScan Mapper with flight lines in different colours; (b) FARO Orbis (red) and YellowScan Mapper (green, local coordinate system) scanning areas.

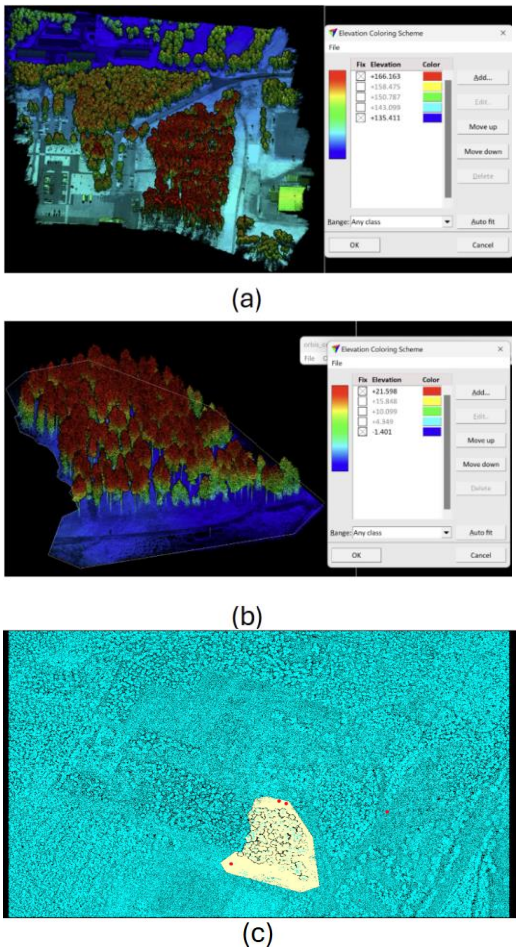

Figure 2. Point clouds obtained with (a) FARO Orbis scanner and (b) YellowScan Mapper coloured by Intensity and elevation in TerraScan. (c) Area scanned by NLS of Finland (navy blue, 5 pts/m2) and FARO Orbis scanner (light yellow). Signal markers are painted with the red dots.

3. Pre-processing point clouds and registration methods

The automated workflow, applied to both ALS and MLS LiDAR-measured point clouds, including the final co-registration step, is summarized in Figure 3. Pre-processing includes splitting trajectories, cutting overlaps between the flight lines (see Figure 1a), smoothing point clouds and removing noise, thinning, classifying ground and above ground objects using the TerraScan macros. The final co-registration is carried out after pre-processing both ALS and MLS data.

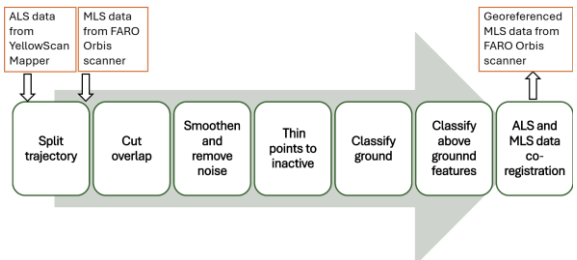

Figure 3. Software-implemented workflow applied to ALS and MLS LiDAR-measured point clouds in the present study.

Both proposed registration methods (by artificial markers and trees) require preliminary ground detection and classifying point clouds (both MLS and ALS) into ground, low, and high vegetation classes. High vegetation corresponds to trees. These steps are elaborated in the next sections.

3.1 Ground point selection and triangulation process

Ground points are initially identified by selecting low-elevation points that are confidently classified as ground hits, based on the absence of buildings within their corresponding 80m×80m grid cell. The process begins with the triangulation stage, where a Triangulated Irregular Network (TIN) model is constructed. Initially, the TIN triangles are positioned below ground level, and in each iteration, an additional ground point is added to the set of ground points.

The iterative process refines the ground classification by determining how close a point must be to an existing triangle plane before it is accepted as a ground point. At each step, the TIN is recomputed using the updated set of ground points, progressively improving the accuracy of the model, see Axelsson (2000).

3.2 Point cloud classification

Following the detection of ground points, the software proceeds to classify the remaining points into three categories: low vegetation, medium vegetation, and high vegetation. This classification is based on an analysis of geometric features, including linearity, anisotropy, change of curvature, sphericity, and verticality (Shcherbacheva et al., 2023), which are computed for each point at multiple scales within individual neighbourhoods of a specified size. Threshold ranges for these statistical features, derived from the typical characteristics of the object classes under consideration, are applied to facilitate accurate classification. The typical values of the geometric features considered for a given class of objects are defined based on elevation.

3.3 Registration with artificial markers

Artificial markers were used as a baseline method for aligning the MLS and ALS data. The ALS dataset, which had centimetre-level georeferencing accuracy, was considered the ground truth for performance evaluation. To ensure precise georeferencing, five GCPs were manually measured.

The software automatically detects GCPs that are located at least 2 m away from trajectories in the MLS data set. Among the detected five GCPs, the user can manually exclude any points that do not match the expected marker shapes. After filtering out false targets, the software uses the 3D coordinates of the remaining GCPs—referenced against ALS measurements—to compute the optimal 3D transformation for the scanned point cloud. Specifically, 2D rotation and translation parameters are estimated by minimizing the residual mismatches between the manually measured reference points and LiDAR-derived points. Two GCPs were employed for computing RMSE of the tested registration methods.

3.4 Tree-Based Registration

3.4.1 Tree Localization and Identification: After classification, individual trees are localized and isolated based on the structural integrity of the point cloud in the ground surface relative to high

vegetation. This approach is justified by the minimal occurrence of laser beam hits within trunk positions. Additionally, tree stems exhibit a systematically homogeneous point distribution across different elevation slices, distinguishing them from other vegetation components and branching structures. These spatial patterns are leveraged to accurately determine individual stem positions.

3.4.2 Registration: Once individual stem locations are identified, a subset of paired stem positions in the ALS dataset is randomly sampled, inspired by the Markov Chain Monte Carlo (MCMC) method. Specifically, 5% of the possible stem pairs are selected for the registration process. A series of experiments has determined the minimum percentage of fixed pairs required to ensure robust registration. This number depends on the total number of stems detected in the ALS data and typically comprises several tens of thousands in practice.

For each pair of ALS stems, a corresponding pair is matched in the MLS dataset based on the criterion that the respective pairwise distances should deviate by no more than 1 meter. Once the matched pairs are identified, a 2D transformation T_i (2D rotation and shift) is computed and applied to the MLS dataset, aligning the MLS stem pair with their ALS counterpart. To assess alignment quality for a given transformation T_i, an alignment metric $Q(T_i)$ is computed:

$$Q(T_i) = \sum_{j=1}^{N} q_j(T_i) \quad , \quad (1)$$

where N is the total number of trees detected in the ALS dataset and $q_j(T_i)$ represents the alignment score for the j-th stem. The individual pairwise alignment metric $q_j(T_i)$ is defined as:

$$q_j(T_i) = \begin{cases} 1, & d_j(T_i) \leq 0.5 \text{ m} \\ 0, & d_j(T_i) > 1.0 \text{ m} \\ \frac{1-d_j(T_i)}{0.5}, & 0.5 < d_j(T_i) \leq 1.0 \text{ m} \end{cases}, \quad (2)$$

where $d_j(T_i)$ denotes the Euclidean distance between the registered stem position for the j -th stem in the ALS dataset and its nearest neighbor in the transformed MLS dataset after applying T_i.
After computing transformations for all randomly sampled fixed stem pairs, the transformation T^* that maximizes $Q(T_i)$ is selected as the optimal one for co-registration:

$$T^* = \arg\max_{T_i} \quad Q(T_i) \quad . \quad (3)$$

Figure 5 demonstrates tree-based alignment. Panels (a)–(c) depict a scenario with fair alignment, where the stem positions in the transformed MLS data closely match those in the ALS reference (see panel (c) for detail). In contrast, panels (d)–(f) show poor alignment, with significant discrepancies between the MLS and ALS stem positions. The left-hand panels display the MLS points—which represent a subset of the ALS points after transformation (see panels (b) and (e))—highlighting that in panel (c) the aligned stems correspond well, while in panel (f) the mismatches are evident.

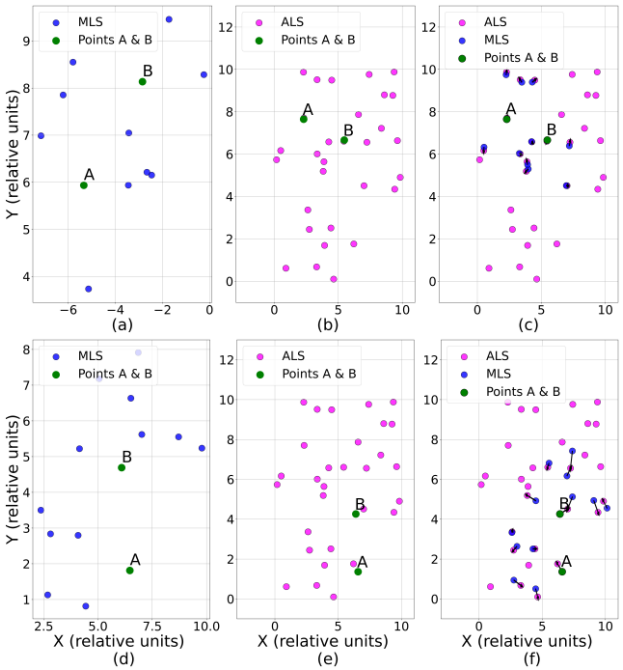

Figure 4. Tree-based registration method illustrated: (a)-(c) Fair alignment and (d)-(f) poor alignment of ALS and MLS point clouds after applying the transformation computed for the pair of points A and B. (a) and (d): MLS points before transformation. (b) and (e): ALS reference points. (c) and (f): MLS points after transformation, aligned with ALS points. In panel (f), nearest neighbours (aligned ALS-MLS stems) are connected by arrows to highlight discrepancies in the alignment.

4. Registration results

Figure 6 presents a visual assessment of the transformed MLS point cloud, generated using two different methods implemented in the software: signal markers and tree trunks. The transformed MLS data is overlaid with the ALS reference dataset to facilitate a comparative evaluation of alignment accuracy. Panels (a) and (c) provide top-down views of the point cloud, allowing for an assessment of the horizontal alignment between the datasets. Panels (b) and (d) show a 1-meter-wide vertical cross-section, where the ALS reference data is represented in yellow and the MLS data in blue, enabling a detailed examination of vertical discrepancies.

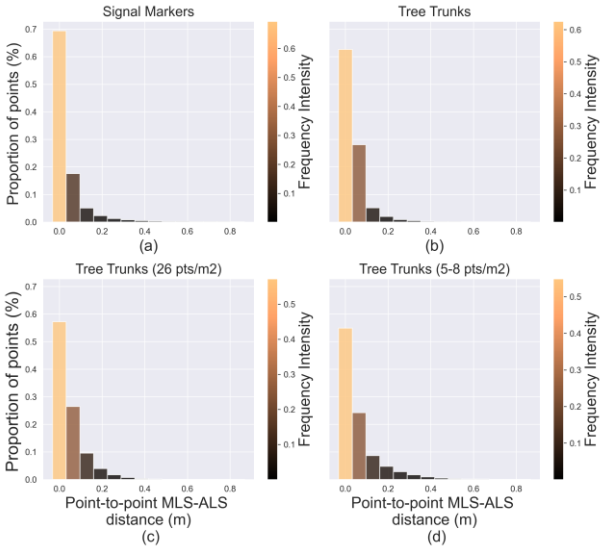

Figure 5. Point-to-point MLS-ALS distance distribution for the applied registration methods: (a) signal markers, tree trunks with (b) 557 pts/m2, (c) 26 pts/m2, and (d) 5-8 pts/m2 ALS resolution.

To quantify the accuracy of each transformation method, the estimated planimetric and altimetric RMSE are summarized in Table 1. Additionally, tree trunk registration with reference data having low spatial resolution is taken into consideration. These error metrics were derived from the differences between ALS reference coordinates and the respective nearest neighbouring points in the transformed MLS point cloud coordinates, providing insight into the relative performance of the two methods. Figure 4 shows a quantitative comparison of point-to-point distances achieved through registration with signal markers and tree trunks using ALS data of varying density (original: 557 pts/m2, 26 pts/m2, 5-8 pts/m2).

As experimental setup testing adaptivity of the methods to density changes in reference ALS data, the ALS data were subsampled from 557 pts/m2 to 26 pts/m2 by density using TerraScan software (with planimetric distance less than 0.8 m used for sub-sampling). Subsequently, the registration procedures were repeated to assess the cross-section view and errors for registration quality.

The histograms computed for registration using a reduced point density (26 pts/m²) and sparse ALS from NLS survey (5-8 pts/m2) showed small differences compared to those generated from the original full density point cloud (557 pts/m²), see Figure 5. Additionally, we test sparse reference ALS data (5 pts/m2) for tree trunk-based registration assessing vertical cross-section view (Figure 7).

For the first registration method based on signal markers, the reference ALS data density does not affect the detection and matching of the markers. Consequently, testing for this type of registration was not conducted, as variations in ALS density do not influence its performance.

As seen in Table 1, most of the mismatches between the reference GCPs and their MLS equivalents occur in altimetry, although matching discrepancies in planimetry are smaller.

Method	**RMSE (m)**		
	Planimetry	Altimetry	Combined
Signal marker	0.013	0.01	0.018
Tree trunks	0.035	0.078	0.087
Tree trunks (26 pts/m2)	0.048	0.074	0.09
Tree trunks (5-8 pts/m2)	0.039	0.064	0.075

Table 1. RMSE of the differences between the estimated point cloud coordinates obtained from FARO Orbis and the manual reference expressed in terms planimetry and altimetry.

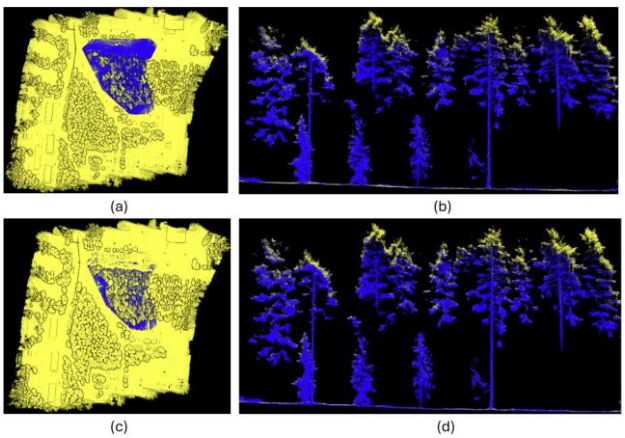

Figure 6. Top views of co-registered ALS-MLS point clouds obtained using (a) signal markers and (c) tree trunks, respectively. (b) and (d): sampled 1 m vertical cross-sections corresponding to (a) and (c), respectively.

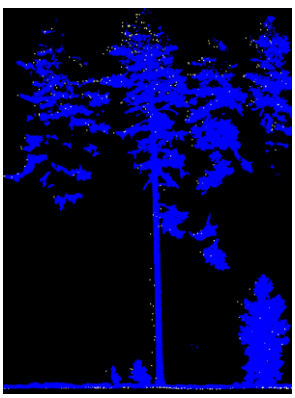

Figure 7. Vertical cross-section (width comprising 1 m) view for NLS of Finland (white, 5 pts/m2) and FARO Orbis (blue) point clouds aligned using tree trunk method.

5. Conclusion

In this study, we demonstrated the capabilities of our software for ALS and MLS data co-registration using data from the FARO Orbis handheld scanner and the YellowScan Mapper UAV-based scanner. Our registration approach achieved an average RMSE of 8.7 cm for tree stem-based co-registration and 2 cm for signal marker-based co-registration. These accuracy levels exceed the accuracy reported in many of the earlier published results. For instance, benchmarked methods specifically designed for forest environments, as well as global methods such as ICP (plane-to-plane) and NDT, achieved alignment accuracy better than 20 cm in both planimetric and altimetric dimensions. Additionally, stem-based methods demonstrated consistent stability across boreal and temperate forest datasets, with Hyyppä et al. (2021) reporting a planimetric RMSE of 12 cm in boreal forest applications, see Campos et al, 2024. The experiments conducted in this study demonstrate that, when comparing transformed MLS point clouds directly to ALS data, over 68% of the points aligned within 15 cm using the tree stem-based method, whereas the signal marker-based alignment achieved a slightly higher accuracy, with 72.2% of points falling within this threshold. These results confirm that our software provides competitive registration accuracy comparable to state-of-the-art methods.

Both registration approaches evaluated offer a universal and automated solution due to software’s ability to pre-classify ALS points into ground, low, medium, and high vegetation with subsequent tree stem detection. This detection leverages the systematic distribution of ground points beneath individual tree canopies, ensuring reliable alignment. Additionally, the registration methods are computationally efficient, utilizing highly optimized multi-threaded CPU processing the rapid co-registration of hundreds of millions of points within seconds. A baseline signal marker-based registration produced RMSE comprising 1.8 cm, while tree trunk-based method with the original YellowScan Mapper point density produced RMSE comprising 8.7 cm.

When the point cloud density of the ALS data has been reduced from 557 pts/m2 to 26 pts/m2, the RMSE comprised 9 cm. Also, the resulting point-to-point MLS-ALS distance distributions displayed no statistical difference, demonstrating high adaptivity to point density deterioration. Additionally, we tested sparse ALS data from NLS of Finland with 5-8 pts/m2 point density covering larger area for tree trunk-based registration and achieved fair vertical cross-section alignment with the MLS point cloud and RMSE comprising 7.5 cm. Centimiter-level variations in the RMSE can be caused by different scanning geometries and random deviations in the measurement procedures. Altimetric alignment may also produce variations because of 2D transformation alignment. Planimetric alignments measure 1.3-4.8 cm, whereas altimetric alignments measure 1-7.8 cm. Statistically tree-trunk based registration is similar regardless of the ALS reference point density.

It is worth noting that airborne scanning has fair GNSS location and can scan treetops, allowing for accurate tree height estimation. Simultaneously, ground-based mobile platforms provide height point cloud density on tree trunks, allowing for the measurement of trunk diameters; however, treetops are frequently inaccessible for these platforms due to dense canopy. If satellites are not visible or there is no GPS sensor present, terrestrial scanning frequently requires a geolocation approach. Co-registering terrestrial and airborne LiDAR data allows for the simultaneous computation of tree height and diameter properties. Overall, our results highlight the effectiveness of the proposed methods, confirming their suitability for high-accuracy forest mapping and ALS-MLS data integration. However, the tree trunk-based registration method has limitations and cannot be used when the point cloud pattern is uniform and there are no point density variations. Also, if MLS data drifts due to poor GNSS location, a simple 3D transformation cannot correct for the misalignment, hence another registration technique must be incorporated in the software.

Acknowledgements

With 36 years of expertise, Terrasolid is the industry standard in point cloud and image processing, delivering high-performance solutions for geospatial, engineering, military, and environmental applications. Its software provides advanced tools for 3D modelling, feature extraction, orthophotos, terrain representation, and point cloud visualization. Supporting all major acquisition platforms (UAV, MLS, ALS, TLS, handheld scanners), it enables Point Cloud Data Fusion from multiple sources.

The Terrasolid suite includes five core products—TerraScan, TerraModeler, TerraPhoto, TerraMatch, and TerraStereo—which can be seamlessly integrated for specific processing tasks and powerful batch processing.

Arttu Soininen (CTO at Terrasolid) has developed and optimized TerraScan’s algorithms, enhancing their efficiency and performance for advanced point cloud processing.

Thanks go to Toby Tang (R&D, AI developer at Terrasolid) for careful proof-reading and suggested corrections.

References

Abayowa, B.O., Yilmaz, A., Hardie, R.C., 2015: Automatic registration of optical aerial imagery to a LiDAR point cloud for generation of city models. *ISPRS J. Photogramm. Remote Sens.*, 106, 68–81.

Avbelj, J., Iwaszczuk, D., Müller, R., Reinartz, P., Stilla, U., 2015: Coregistration refinement of hyperspectral images and DSM: An object-based approach using spectral information. *ISPRS J. Photogramm. Remote Sens.*, 100, 23–34.

Axelsson, P., 2000: DEM generation from laser scanner data using adaptive TIN models. *ISPRS Int. Arch. Photogramm. Remote Sens. Spatial Inf. Sci.*, 33, 110-117.

Bastos, A., Hasegawa, H., 2013: Behavior of GPS signal interruption probability under tree canopies in different forest conditions. *Eur. J. Remote Sens.*, 46, 613-622. doi.org/10.5721/EuJRS20134636.

Benson, M.L., Pierce, L., Bergen, K., Sarabandi, K., 2020: Model-based estimation of forest canopy height and biomass in the Canadian boreal forest using radar, LiDAR, and optical remote sensing. *IEEE Trans. Geosci. Remote Sens.*, 59, 4635–4653.

Best, P.J., McKay, N.D., 1992: A method for registration of 3-D shapes. *IEEE Trans. Pattern Anal. Mach. Intell.*, 14, 239–256.

Campos, M.B., Castanheiro, L.F., Shah, D., Wang, Y., Kukko, A., Puttonen, E., 2024: Overview and benchmark on multi-modal LiDAR point cloud registration for forest applications. *ISPRS Int. Arch. Photogramm. Remote Sens. Spatial Inf. Sci.*, XLVIII-1-2024, 43–50. doi.org/10.5194/isprs-archives-XLVIII-1-2024-43-2024.

Castanheiro, L.F., Tommaselli, A.M.G., Garcia, T.A.C., Campos, M.B., Kukko, A., 2023: Point cloud registration using laser data from an orange orchard. *ISPRS Int. Arch. Photogramm. Remote Sens. Spatial Inf. Sci.*, 48, 71-77.

Chen, J., Zhao, D., Zheng, Z., Xu, C., Pang, Y., Zeng, Y., 2024: A clustering-based automatic registration of UAV and terrestrial LiDAR forest point clouds. *Comput. Electron. Agric.*, 217, 108648.

Cheng, X., Liu, X., Huang, Y., Zhou, W., Nie, J., 2024: Efficient registration of airborne LiDAR and terrestrial LiDAR point clouds in forest scenes based on single-tree position consistency. *Forests*, 15(12), 2185.

Dai, W., Yang, B., Liang, X., Dong, Z., Huang, R., Wang, Y., Li, W., 2019: Automated fusion of forest airborne and terrestrial point clouds through canopy density analysis. *ISPRS J. Photogramm. Remote Sens.*, 156, 94–107.

Ester, M., Kriegel, H.P., Sander, J., Xu, X., 1996: A density-based algorithm for discovering clusters in large spatial databases with noise. *Proc. 2nd Int. Conf. on Knowledge Discovery and Data Mining*, United States.

Guo, Q., Liu, J., Tao, S., Xue, B., Li, L., Xu, G., Li, W., Wu, F., Li, Y., Chen, L., 2014: Perspectives and prospects of LiDAR in forest ecosystem monitoring and modeling. *Chin. Sci. Bull.*, 59, 459–478.

Hauglin, M., Lien, V., Næsset, E., Gobakken, T., 2014: Geo-referencing forest field plots by co-registration of terrestrial and airborne laser scanning data. *Int. J. Remote Sens.*, 35, 3135–3149.

Hohenthal, J., Alho, P., Hyyppä, J., Hyyppä, H., 2011: Laser scanning applications in fluvial studies. *Prog. Phys. Geogr.*, 35, 782–809.

Hyyppä, E., Muhojoki, J., Yu, X., Kukko, A., Kaartinen, H., Hyyppä, J., 2021: Efficient coarse registration method using translation- and rotation-invariant local descriptors towards fully automated forest inventory. *ISPRS Open J. Photogramm. Remote Sens.*, 2, 100007.

Kelbe, D.; Van Aardt, J.; Romanczyk, P.; Van Leeuwen, M.; Cawse-Nicholson, K., 2015: Single-scan stem reconstruction using low resolution terrestrial laser scanner data. *IEEE J. Sel. Top. Appl. Earth Obs. Remote Sens.*, 8, 3414–3427.

Kukkonen, M.; Maltamo, M.; Korhonen, L.; Packalen, P., 2021: Fusion of crown and trunk detections from airborne UAS based laser scanning for small area forest inventories. *Int. J. Appl. Earth Obs. Geoinf.*, 100, 102327.

Liang, L.X.; Hyyppä, J., 2013: Automatic stem mapping by merging several terrestrial laser scans at the feature and decision levels. *Sensors*, 13, 1614–1634.

Liang, X.; Hyyppä, J.; Kaartinen, H.; Lehtomäki, M.; Pyörälä, J.; Pfeifer, N.; Holopainen, M.; Brolly, G.; Francesco, P.; Hackenberg, J., 2018: International benchmarking of terrestrial laser scanning approaches for forest inventories. *ISPRS J. Photogramm. Remote Sens.*, 144, 137–179.

Liu, L.; Pang, Y.; Li, Z., 2016: Individual tree DBH and height estimation using terrestrial laser scanning (TLS) in a subtropical forest. *Sci. Silvae Sin.*, 52, 26–37.

Liu, J., Liang, X., Hyyppä, J., Yu, X., Lehtomäki, M., Pyörälä, J., Zhu, L., Wang, Y., Chen, R., 2017a: Automated matching of multiple terrestrial laser scans for stem mapping without the use of artificial references. *Int. J. Appl. Earth Obs. Geoinf.*, 56, 13–23.

Liu, L.; Pang, Y.; Li, Z.; Si, L.; Liao, S., 2017b: Combining airborne and terrestrial laser scanning technologies to measure forest understorey volume. *Forests*, 8, 111.

Liu, Q.; Ma, W.; Zhang, J.; Liu, Y.; Xu, D.; Wang, J. Point-cloud segmentation of individual trees in complex natural forest scenes based on a trunk-growth method. *J. For. Res.* 2021, 32, 2403–2414.

Mori, A.S., Lertzman, K.P., Gustafsson, L., 2017: Biodiversity and ecosystem services in forest ecosystems: A research agenda for applied forest ecology. *J. Appl. Ecol.*, 54, 12–27.

Pang, Y., Zhao, F., Li, Z., 2008: Forest height inversion using airborne LiDAR technology. *J. Remote Sens.*, 12, 158.

Paris, C.; Kelbe, D.; Van Aardt, J.; Bruzzone, L.: 2017: A novel automatic method for the fusion of ALS and TLS LiDAR data for robust assessment of tree crown structure. *IEEE Trans. Geosci. Remote Sens.*, 55, 3679–3693.

Pohjavirta, O., Liang, X., Wang, Y., Kukko, A., Pyörälä, J., Hyyppä, E., Hyyppä, J., 2022: Automated registration of wide-baseline point clouds in forests using discrete overlap search. *Forest Ecosystems*, 9, 100080.

Polewski, P.; Erickson, A.; Yao,W.; Coops, N.; Krzystek, P.; Stilla, U., 2016: Object-based coregistration of terrestrial photogrammetric and ALS point clouds in forested areas. *ISPRS Ann. Photogramm. Remote Sens.* Spat. Inf. Sci., 3, 347–354.

Polewski, P.; Yao, W.; Cao, L.; Gao, S., 2019: Marker-free coregistration of UAV and backpack LiDAR point clouds in forested areas. *ISPRS J. Photogramm. Remote Sens*., 147, 307–318.

Pueschel, P., 2013: The influence of scanner parameters on the extraction of tree metrics from FARO Photon 120 terrestrial laser scans. *ISPRS J. Photogramm. Remote Sens.*, 78, 58–68.

Puletti, N.; Grotti, M.; Masini, A.; Bracci, A.; Ferrara, C., 2022: Enhancing wall-to-wall forest structure mapping through detailed co-registration of airborne and terrestrial laser scanning data in Mediterranean forests. *Ecol. Inform.*, 67, 101497.

Shao, J., Yao, W., Wan, P., Luo, L., Wang, P., Yang, L., Lyu, J., Zhang, W., 2022: Efficient co-registration of UAV and ground LiDAR forest point clouds based on canopy shapes. *International Journal of Applied Earth Observation and Geoinformation,* 114, 103067.

Shcherbcheva, A., Campos, M.B., Liang, X., Puttonen, E., Wang, Y., 2023: Unsupervised statistical approach for tree-level separation of foliage and non-leaf components from point clouds. *ISPRS Int. Arch. Photogramm. Remote Sens. Spatial Inf. Sci.*, XLVIII-1/W2-2023, 1787-1794. doi.org/10.5194/isprs-archives-XLVIII-1-W2-2023-1787-2023.

Tremblay, J.-F., Béland, M., 2018: Towards operational marker-free registration of terrestrial LiDAR data in forests. *ISPRS J. Photogramm. Remote Sens.*, 146, 430–435.

Wehr, A., Lohr, U., 1999: Airborne laser scanning—An introduction and overview. *ISPRS J. Photogramm. Remote Sens.*, 54, 68–82.

Yang, M.Y., Cao, Y., McDonald, J.: 2011: Fusion of camera images and laser scans for wide baseline 3D scene alignment in urban environments. *ISPRS J. Photogramm. Remote Sens.*, 66, S52–S61.

Zhang, W.; Chen, Y.; Wang, H.; Chen, M.; Wang, X.; Yan, G., 2016: Efficient registration of terrestrial LiDAR scans using a coarse-to-fine strategy for forestry applications. *Agric. For. Meteorol.*, 225, 8–23.

Zhang, W.; Li, D.; Chen, Y.; Shao, J.; Shen, A.; Yan, G., 2018: Integration between TLS and UAV photogrammetry techniques for retrieving tree height. *Beijing Norm. Univ. (Nat. Sci.)*, 54, 764–771.

Zhang, W., Shao, J., Jin, S., Luo, L., Ge, J., Peng, X., Zhou, G., 2021: Automated marker-free registration of multisource forest point clouds using a coarse-to-global adjustment strategy. *Forests*, 12, 269.

Zhou, R.; Sun, H.; Ma, K.; Tang, J.; Chen, S.; Fu, L.; Liu, Q., 2023: Improving estimation of tree parameters by fusing ALS and TLS point cloud data based on canopy gap shape feature points. *Drones*, 7, 524. *Photogramm. Remote Sens. Spatial Inf. Sci.*, IV-1/W1, 215-222. doi.org/10.5194/isprs-annals-IV-1-W1-215-2017.

Michalis, P., Dowman, I., 2008: A Generic Model for Along-Track Stereo Sensors Using Rigorous Orbit Mechanics. *Photogrammetric Engineering & Remote Sensing* 74(3), 303-309.

Smith, J., 1987a. Close range photogrammetry for analyzing distressed trees. *Photogrammetria*, 42(1), 47-56.

Smith, J., 1987b. Economic printing of color orthophotos. Report KRL-01234, Kennedy Research Laboratories, Arlington, VA, USA.

Smith, J., 2000. Remote sensing to predict volcano outbursts. *Int. Arch. Photogramm. Remote Sens. Spatial Inf. Sci.*, XXVII-B1, 456-469.